International Journal of Engineering Research and Science & Technology

ANFIS-Based Soft-Switching V2V Energy Transfer Topology for Enhanced Efficiency in Electric Vehicles

Mrs. Sadhu Renuka[1], P. Tejasri[2], S. Tousif[3], K.Mahammad Meharaan[4]
[1]Assistant Professor, Department of EEE, AITS, Kadapa
[2,3,4] Student (UG), Department of EEE, AITS, Kadapa

Abstract –
One of the most encouraging ways to decrease transportation-related emissions is the electrification of automobiles. The broad adoption of electric vehicles (EVs) is hindered, however, by range anxiety. In times of crisis, the "last-mile" problem can be solved and range anxiety reduced with the help of vehicle-to-vehicle (V2V) energy transfer. However, optimizing efficiency during power transfer is usually overlooked by traditional V2V energy-sharing solutions that rely on motor inverters and motor windings. A novel V2V power-transfer topology with a soft-switching method working at a lower switching frequency is proposed in this research to enhance overall system performance. The motor's windings and silicon-steel core act as an inductive component during V2V energy exchange, and the core losses are greatly reduced by the decreased switching frequency. In addition, the suggested architecture incorporates an ANFIS controller for smart, real-time optimization of switching settings. The ANFIS controller increases energy-transfer efficiency, soft-switching performance, and switching losses by learning nonlinear system features and adjusting to changing operating circumstances and loads. Utilizing a 150-kW simulation model and a 1.5-kW laboratory-scale experimental prototype, the efficacy of the suggested V2V topology with ANFIS-based control is confirmed. The results show enhanced efficiency, decreased core losses, and strong flexibility in various operating situations.

I. INTRODUCTION

Achieving carbon neutrality may be achieved by the combination of electrifying vehicles and generating electricity from renewable sources. Concerns about having insufficient power during longer electronic vehicle (EV) trips and a lack of convenient charging stations continue to slow down widespread adoption of EVs [1]. An effective solution to range anxiety and dependency on public charging infrastructure can be found through vehicle-to-vehicle (V2V) energy transfer, in which a high-energy EV supplies electricity to a low-energy EV. This can be useful in emergency or unforeseen scenarios [2]. We may generally classify the existing V2V energy-sharing techniques into three groups [3]. In the first group, energy may be transferred between cars by means of external, or off-board, chargers. In [4], for instance, a single-phase bridgeless converter is suggested for use as an off-board charger; in [5], an external charger based on a bidirectional buck-boost converter is introduced. Isolated DC/DC converters, including the dual active bridge (DAB) [6] and CLLC converters [7], are further alternatives to on-board solutions. Also, in [8], it is said that a 75 kW mobile charging infrastructure for EVs is available

for business use. While off-board chargers do allow for flexible V2V power transfer, they aren't viable for broad deployment due to their high system cost, extra weight, and space requirements. The use of bidirectional onboard chargers (OBCs) is the second type of vehicle-to-vehicle energy transfer. To facilitate power transmission between EVs, the single-phase inverter of an OBC is utilized in [9]. Directly linking the two isolation stages can minimize the number of conversion stages and enhance efficiency [10]. This is because conventional OBCs comprise of two power-conversion stages: an isolated DC/DC converter and an inverter. In addition, isolated converters can be replaced with non-isolated bidirectional buck-boost (BBB) converters, which can reduce costs. But traditional OBCs typically have a maximum power rating of about 7.4 kW, which means they have to charge for a long period, which isn't viable for V2V power-sharing emergencies. Another potential method for vehicle-to-vehicle energy transmission is wireless power transfer (WPT). In order to alleviate concerns about range and charging infrastructure constraints, the idea of wireless power transmission between vehicles has been investigated [11]. Nevertheless, coil alignment, transmission distance, and positioning precision are limitations of existing WPT-based V2V systems. Due to its impracticality and the fact that coil misalignment drastically reduces power-transfer efficiency, WPT is not a good fit for V2V applications that require a lot of power and time-sensitive data transmission [12]. The third type of vehicle-to-vertical energy exchange systems use converters that are hardwired into the electric vehicle's battery. There are often two setups. Type II involves a direct connection between the battery and the motor inverter, whereas Type I involves the insertion of a bidirectional buck-boost (BBB) converter. A bidirectional DC/DC converter for V2V energy transmission is formed in [13] by connecting two BBB converters with an extra capacitor. Nevertheless, with just two switches, the transferable power is limited, and the system cost and complexity are also increased. In order to overcome these constraints, a control method that is based on the Type I converter is suggested in [14]. This technique involves reducing conduction losses through energy transfer that involves the motor inverter and windings. Type I arrangement has several benefits, but high-current inductors and switching devices are expensive and bulky, so it's not always practical.

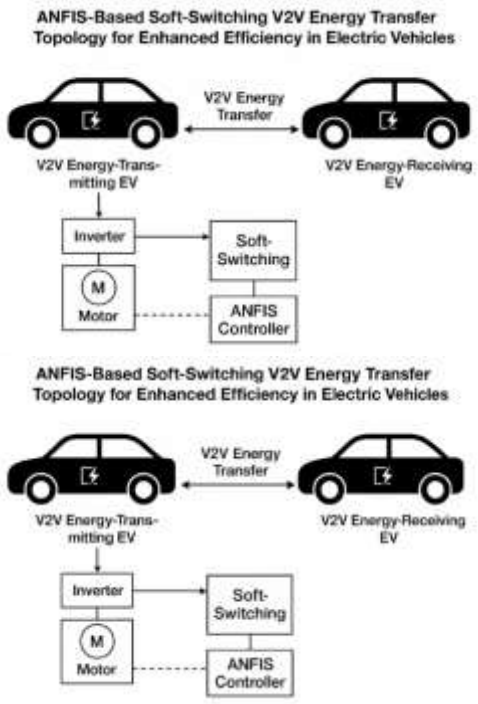


Fig 1. Block Diagram of the Proposed concept.

Because they need so little in the way of hardware, Type II arrangements are becoming more popular. This method

involves converting the motor windings into inductive components and using the motor inverter as a power transfer rectifier or inverter. But mechanical locking mechanisms are required because the motor windings produce unwanted electromagnetic torque when sinusoidal currents run through them. Although methods for circuit reconfiguration have been suggested in to do away with torque production, these solutions are inefficient since they necessitate more mechanical or electronic switches and include more power-conversion stages. Although new power electronic components are required for torque-free V2V topologies, they are also documented. In addition, the switching frequencies used by current Type II-based V2V systems are often rather high, such as 20 kHz and 15 kHz. The fact that stators used in electric vehicle motors are often made of silicon steel—whose ideal operating frequency is often lower than 10 kHz —is ignored in this. The efficiency of V2V energy transfer is greatly diminished while operating at high frequencies because the motor windings experience substantial core losses.

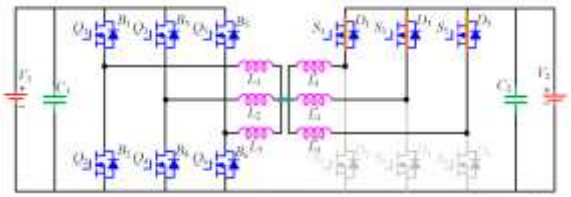


Fig. 2. The circuit with the proposed control method.

In order to get past these obstacles, this study suggests a new V2V energy-transfer architecture that uses a Type II battery-inverter setup. The suggested architecture just calls for one stage of power conversion and doesn't call for any supplementary hardware. To decrease switching losses and motor stator core losses, a torque-free soft-switching control approach is designed with lower switching frequency. Also included is a controller that uses an Adaptive Neuro-Fuzzy Inference System (ANFIS) to optimize the switching parameters intelligently in real time for different types of operations. Improved efficiency, decreased losses, and significant flexibility for V2V energy-transfer applications are demonstrated by a 1.5 kW laboratory-scale experimental prototype and a 150 kW simulation model, respectively, proving the efficacy of the suggested method.

II. PROPOSED V2V TOPOLOGY AND OPERATION PRINCIPLE

A. Proposed V2V Topology

In Fig. 2, we can see the suggested V2V energy-transfer topology in action, with the electric car motor inverter and motor windings utilized. Through their respective charging ports, a specialized V2V cable links the two EVs. The neutral points of the three-phase motor windings in both electric vehicles are linked through the L1 and L′1 ports, however the charging interfaces' negative DC terminals (DC−) are linked directly.

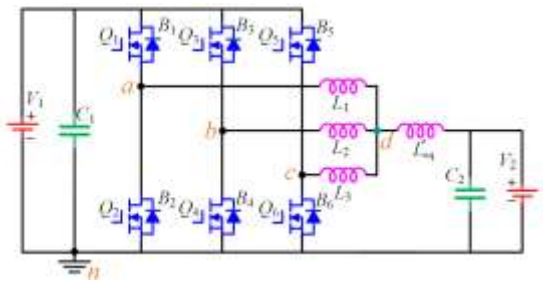


Fig. 3. The simplified equivalent circuit with the proposed control method. Where in, L′ eq=L′ 1//L′ 2//L′ 3. And, van, vbn, vcn, and vdn are node voltage produced according to the label in this figure.

International Journal of Engineering Research and Science & Technology

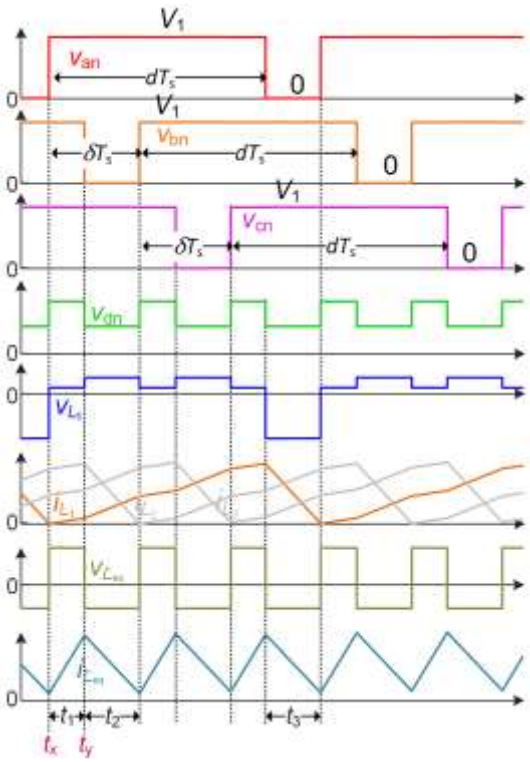


Fig. 4. Waveforms of the inductor voltage and current of interleaved control. Here, phase shift ratio δ=1/3

The suggested design allows V2V power sharing without the need for extra mechanical switches or circuit reconfiguration, which is a major advantage. Eliminating the need to incorporate additional power electronic components reduces system complexity and expense, as the motor inverter and motor windings are already present in EVs. using the use of suitable control protocols, it is possible to realize communication between the two cars and to select a V2V charging mode using the already existing charging interfaces. Type I converter designs are also compatible with the suggested topology, even though it is mostly based on Type II battery-inverter configurations. In a Type I arrangement, as described, a CLC filter is placed between the electric vehicle battery and the motor inverter, and the upper and lower switches of the bidirectional buck-boost (BBB) converter are kept continually on. The V2V operation is unaffected by the peripheral battery-side circuitry due to the fact that the suggested control approach and architecture primarily address the motor inverter and windings. So, Type I and Type II converter designs are both compatible with the suggested method. It should be mentioned that there's no way to ensure compatibility with every single electric vehicle model. Although motor inverters are common in electric vehicles, the suggested architecture need an outside source to reach the motor windings' neutral point. Because of this, connecting the motor to the charging interface requires an extra wire. Accordingly, the design of the vehicle's motor and charging system determines the implementation's practicality. Additionally, the lower-rated vehicle limits the maximum transferred power when the two cars have differing power ratings. The voltage that an electric vehicle's battery can handle is limited by the operational voltage range of lithium-ion cells, which is 2.75 to 4.2 V for 18650 cells. Around 275 V could be the bare minimum for a 400 V EV system's batteries. This analysis runs under the assumption that the low-energy EV operates at 275 V and the high-energy EV at 400 V, based on realistic V2V energy-sharing scenarios. This is the circumstance under which all further analyses are carried out.

B. Voltage Gain Derivation

Using a three-phase interleaved parallel control technique, the suggested topology enables several switches to conduct power in parallel, therefore reducing conduction losses. One motor inverter is controlled by three-phase interleaved circuits, whereas

the inverter on the other side has one set of switches that are always ON. Figure 3 shows the resultant circuit layout when using this control mechanism. In buck-mode operation, power moves from the left side to the right side, supposing V1>V2. Here, the left-side inverter is controlled by interleaved modulation, and switches S1, S3, and S5 stay ON all the time. By inverting Figure 3 horizontally, the circuit may be produced for boost-mode operation (V1<V2). Switches Q1, Q3, and Q5 stay on in this mode, and the right-side inverter is regulated by interleaved modulation. An important benefit of interleaved parallel control is that it reduces output voltage ripple by increasing the effective frequency of the current flowing into the DC-link capacitor.

For voltage-gain analysis, a simplified equivalent circuit is shown in Fig. 4, where $L'_{eq} = L'_1 \parallel L'_2 \parallel L'_3$ represents the equivalent inductance of the motor windings. Simulation results indicate that the current through L'_{eq} equals the sum of the phase currents, and its ripple frequency is three times the switching frequency due to interleaved operation.

Applying the volt–second balance principle to L'_{eq}, the voltage gain of the converter can be derived. Following the detailed derivation shown in (1)–(7), the voltage gain in buck mode is given by

$$m = \frac{V_2}{V_1} = d$$

and the voltage gain in boost mode is

$$m_{bo} = \frac{1}{d}$$

C. Zero-Torque Operating Condition

During power transfer, the motor must not produce electromagnetic torque; this is a basic condition of the suggested V2V topology. The quickest approach to meet this requirement is to keep the motor winding current minimum above zero. At this state, the stator core contains just a direct current magnetic field, which means that the average torque is zero. Because it is controlled by three phases interleaved, the ripple current of L'_{eq} is much lower than that of the individual phase inductors L1, L2, and L3. Therefore, L'_{eq} minimum current will likewise be positive if the minimum current of each phase inductor stays positive. The link between output power and switching frequency may be obtained by studying the relationships between the inductor voltage and current using Kirchhoff's voltage law and the volt-second balance principle.

$$P_o = \frac{V_2(V_1 - V_2)(2V_1 + 3V_2)}{4V_1 L_1 f_s}$$

This expression indicates that, for fixed voltages and inductance, output power increases as switching frequency decreases. Since EV motor stator cores are typically designed to operate at several hundred hertz, low-frequency operation significantly reduces core losses. Therefore, variable-frequency control is essential to achieve zero-torque operation over a wide output power range.

D. Zero-Voltage-Switching (ZVS) Condition Analysis

With appropriate control, the proposed topology enables zero-voltage switching (ZVS) for all power devices. Taking switch pair Q_1–Q_2 as an example, the ZVS operation is analyzed using the waveforms the operating modes illustrated.

To achieve ZVS, the parasitic output capacitance of the switch must be fully discharged during the dead time. This leads to the following conditions:

$$i_{L1,\min} < -\frac{2V_1 C_{oss}}{t_D}$$

$$i_{L1,\max} > \frac{2V_1 C_{oss}}{t_D}$$

With typical system parameters, the required negative current for ZVS is very small and introduces negligible torque due to the large DC bias of the inductor current. Therefore, ZVS can be achieved without compromising torque-free operation.

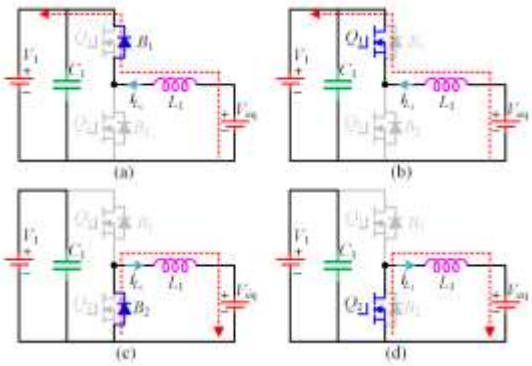


Fig. 5. Operating mode of ZVS.

III. PROPOSED CONTROL METHOD WITH ANFIS AND SIMULATION RESULTS

To implement the suggested V2V energy-transfer topology, a control method is needed that can provide zero-voltage-switching (ZVS), zero-torque operation, and high efficiency under different operating situations. Due to the continual variation in battery voltages, load power demands, and motor winding characteristics, control solutions based on fixed parameters or pure analysis are inadequate for real-world V2V scenarios. We present a control technique based on the Adaptive Neuro-Fuzzy Inference System (ANFIS) to optimize the switching frequency and current bias intelligently in real-time in order to overcome these obstacles. The results of the Section II study clearly show that the output power is highly dependent on the switching frequency, battery voltages, and inductance of the motor windings. The ideal value of the regulated negative current bias, which is necessary for ZVS, changes depending on the parasitic characteristics of the device and the output power. Due to these linked nonlinear connections, traditional controllers based on PI or rules are less resilient to changes in parameters and more complex to adjust.

A. ANFIS-Based Control Architecture

To overcome these limitations, an ANFIS-based controller is integrated into the proposed control framework. The ANFIS combines fuzzy logic reasoning with neural network learning capability, enabling adaptive control of nonlinear systems with uncertain and time-varying parameters. It illustrates the overall control architecture. The ANFIS controller receives real-time system measurements as inputs, including:

- battery voltages V_1 and V_2;
- output power reference P_o^*;
- measured output power P_o;
- estimated motor winding inductance L_1.

Based on these inputs, the ANFIS generates two key control outputs:

1. the optimal switching frequency f_s;
2. the reference minimum inductor current $i_{L1,\min}^*$, which introduces a controlled negative bias to guarantee ZVS.

The duty cycle is calculated analytically from the voltage-gain relationship derived in Section II-B, while the ANFIS focuses on optimizing frequency and current bias to satisfy multiple performance objectives simultaneously.

B. ANFIS Structure and Training Process

The adopted ANFIS structure is based on a first-order Sugeno fuzzy inference system. Each input variable is assigned a set of membership functions, and fuzzy rules are constructed to capture the nonlinear relationship between operating conditions and optimal control parameters. During the offline training phase, datasets are generated using analytical expressions derived in Section II and validated through detailed simulations. The training data include various combinations of battery voltages, power levels, and inductance variations. The target outputs are the optimal switching frequency and minimum inductor current that ensure:

- zero-torque operation,
- ZVS for all switches,
- minimal switching and core losses,
- acceptable output voltage ripple.

The hybrid learning algorithm, which combines least-squares estimation and gradient descent, is used to adjust membership function parameters and rule weights. After training, the ANFIS controller is implemented online with minimal computational overhead, making it suitable for real-time EV applications.

C. Variable-Frequency Control and Voltage Ripple Constraint

As derived in Section II-D, reducing the switching frequency increases output power capability and decreases motor core losses. However, excessive reduction in switching frequency results in increased output voltage ripple. The output voltage ripple is expressed as

$$\Delta V_2 = \frac{(3V_2-2V_1)(V_1-V_2)}{48C_2L_1V_1f_s^2}$$

To balance efficiency and voltage quality, the ANFIS controller adaptively adjusts the switching frequency to the minimum value that satisfies a predefined voltage ripple limit. Compared to fixed-frequency operation, this adaptive strategy ensures that the system always operates near the optimal efficiency point.

D. ZVS Optimization Using ANFIS

ZVS conditions derived in Section II-D impose minimum and maximum limits on the inductor current. These limits vary with switching frequency, output power, and device parasitic capacitance. Instead of using a conservative fixed current bias, the ANFIS controller dynamically adjusts the minimum inductor current reference as a small percentage of the peak current:

$$i^*_{L1,\min} = -k \cdot i_{L1,\max}$$

where $k$is adaptively determined by the ANFIS.

This adaptive ZVS strategy ensures reliable soft switching across the entire operating range while minimizing unnecessary circulating current, thereby reducing conduction losses.

E. Proposed Control Block Diagram with ANFIS Integration

Based on the analytical derivations and simulation validation, the overall control block diagram of the proposed V2V system. The proposed control strategy is fundamentally a constant-power controller composed of two coordinated control loops: a duty-cycle control loop and a switching-frequency control loop. To enhance adaptability and robustness under varying operating conditions, an Adaptive Neuro-Fuzzy Inference System (ANFIS) is integrated into the switching-frequency control layer.

1) Duty-Cycle Control Loop

The duty-cycle controller regulates the instantaneous power flow between the two

EVs. The reference charging power $P_{o,\text{ref}}$ is converted into a reference charging current $I_{o,\text{ref}} = \frac{P_{o,\text{ref}}}{V_2}$,
where $V_2$is the battery voltage of the receiving EV. A closed-loop PI controller compares the measured charging current $I_o$with $I_{o,\text{ref}}$ and adjusts the duty cycle accordingly. By controlling the duty cycle, the voltage difference between the converter output and the battery voltage is regulated, thereby indirectly controlling the charging current and achieving constant-power operation. This duty-cycle control loop relies only on local measurements of $V_2$and I_o, enabling fast dynamic response and stable power regulation.

2) ANFIS-Based Switching-Frequency Control Loop

The second component of the control system determines the switching frequency, which plays a critical role in ensuring zero-torque operation, ZVS, and minimized motor core losses. As derived, the output power is inversely proportional to the switching frequency for given battery voltages and inductance values. However, in practical V2V scenarios, battery voltages $V_1$and V_2, motor winding inductance, and output power demand vary continuously, making fixed-frequency or purely analytical control inadequate. To address this challenge, an ANFIS-based controller is employed to determine the optimal switching frequency in real time. The ANFIS takes the following variables as inputs:

- measured battery voltages $V_1$and V_2;
- reference output power $P_{o,\text{ref}}$;
- estimated motor winding inductance L_1.

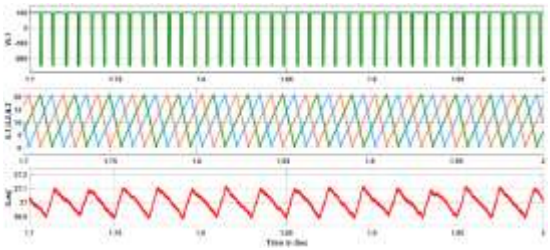
Based on these inputs, the ANFIS outputs the optimal switching frequency f_s, which satisfies three constraints simultaneously:

1. the output voltage ripple remains within the specified limit;
2. the minimum inductor current ensures ZVS operation;
3. the switching frequency is minimized to reduce motor stator core loss.

A critical operating condition occurs when V_1 approaches V_2. As shown, the analytically calculated power transfer capability tends toward zero under this condition, leading to an unrealistically low switching frequency. To avoid this issue, a minimum switching frequency threshold $f_{s,\text{min}}$is enforced. When the ANFIS output reaches this limit, power regulation is smoothly transferred to the duty-cycle control loop, ensuring continuous and stable power transfer.

V. SIMULATION RESULTS

In this study, detailed simulations are first conducted to verify the derived analytical expressions and to support the design of the proposed control method. By substituting the parameters V_1, V_2, C_2, L_1, and the output voltage ripple requirement ΔV_2listed into the theoretical minimum switching frequency can be calculated. For an output voltage ripple constraint of 3 V, the minimum switching frequency is obtained as 192.77 Hz.



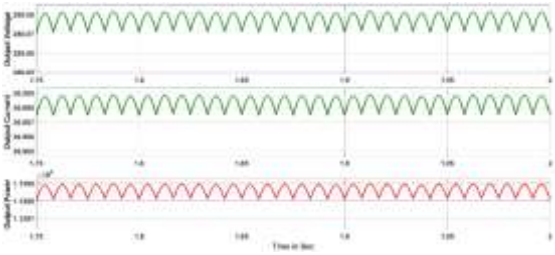
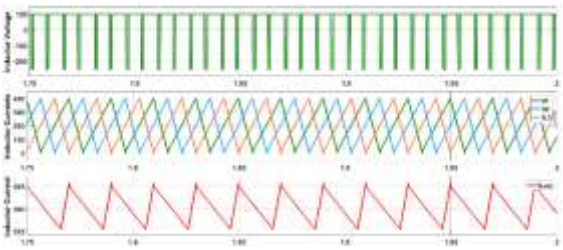
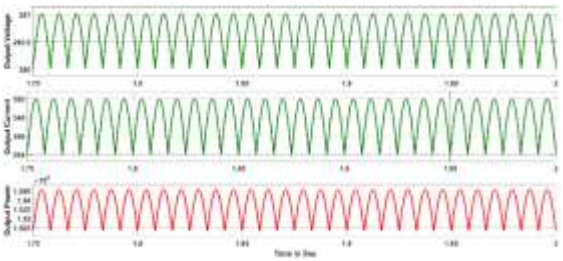


Fig. 6. Simulation waveforms with 10kW, fs=3.1kHz.



(a)



(b)

Fig. 7. Simulation waveforms with 150kW, fs=202Hz.

To enable comparison with existing high-power V2V methods reported in the literature, the simulation power range is set from 10 kW to 150 kW, corresponding to a switching-frequency range of pproximately 3.1 kHz to 220 Hz. The typical EV system parameters used in the simulation are summarized. Fig. 6 shows the simulation waveforms obtained from PLECS under two representative operating conditions: 10 kW and 150 kW. As shown in Fig. 7(a), when the output power is 10 kW and the switching frequency is 3.1 kHz, the output voltage ripple remains well below the specified 3-V limit. Fig. 7(b) illustrates the high-power operating condition at 150 kW with a switching frequency of approximately 202 Hz, where the output voltage ripple still satisfies the design requirement. The minimum values of the phase inductor currents i_{L1}, i_{L2}, and $i_{L3}$are −1.1 A at 10 kW and −4.1 A at 150 kW, respectively. These values closely match the analytically determined reference minimum current required for ZVS operation, validating the accuracy of the theoretical analysis and confirming that torque-free operation and ZVS can be achieved simultaneously over a wide power range.

CONCLUSION

This paper presented an ANFIS-based soft-switching vehicle-to-vehicle (V2V) energy-transfer topology aimed at improving energy-transfer efficiency and operational robustness in electric vehicles. By leveraging the existing motor inverter and motor windings, the proposed topology enables high-power V2V energy sharing without introducing additional hardware, thereby maintaining compactness and cost effectiveness. A reduced switching-frequency soft-switching strategy was employed to significantly minimize switching losses and motor core losses during V2V operation. To address the nonlinear and time-varying characteristics of battery voltages, load conditions, and motor parameters, an Adaptive Neuro-Fuzzy Inference System (ANFIS) controller was integrated into the switching-frequency control loop. The ANFIS controller provides real-time optimization of switching frequency while ensuring output voltage ripple constraints and zero-voltage-switching (ZVS) conditions are satisfied over a wide power range. The proposed control method was validated through a 150-kW simulation model and a 1.5-kW laboratory-scale experimental

prototype. Both simulation and experimental results demonstrate that the proposed topology achieves stable constant-power control, reduced voltage ripple, and effective torque-free operation under varying operating conditions. Compared with conventional V2V energy-transfer methods, the proposed ANFIS-based control strategy exhibits enhanced efficiency, reduced core losses, and improved adaptability, making it a promising solution for emergency energy sharing and last-mile support in electric vehicle applications.

REFERENCES

[1] C. C. Chan, "The state of the art of electric, hybrid, and fuel cell vehicles," *Proc. IEEE*, vol. 95, no. 4, pp. 704–718, Apr. 2007.

[2] J. M. Miller, K. T. Chau, and O. C. Onar, "Vehicle-to-vehicle and vehicle-to-grid energy transfer: Opportunities and challenges," *IEEE Trans. Power Electron.*, vol. 31, no. 7, pp. 4903–4913, Jul. 2016.

[3] Immadi, S. K. (2025). Optimizing ERP for Human Capital Management. Applied Research for Growth, Innovation and Sustainable Impact, 377–384. https://doi.org/10.1201/9781003684657-63.

[4] Mahesh Ganji. (2025). Enhancing Oracle Cloud HR Reporting Through AI-Driven Automation. Journal of Science & Technology, 10(6), 28–36. https://doi.org/10.46243/jst.2025.v10.i06.pp28-36.

[5] M. Yilmaz and P. T. Krein, "Review of charging power levels and infrastructure for plug-in electric and hybrid vehicles," *IEEE Trans. Power Electron.*, vol. 28, no. 5, pp. 2151–2169, May 2013.

[6] Snigdha Gaddam. (2025). SOFTWARE STACK PREPARED FOR AI TRANSITIONING FROM MODULES TO MODELS. American Journal of AI Cyber Computing Management, 5(4), 451–462. https://doi.org/10.64751/ajaccm.2025.v5.n4.pp451-462.

[7] R. W. Erickson and D. Maksimović, *Fundamentals of Power Electronics*, 2nd ed. New York, NY, USA: Springer, 2001.

[8] J. A. Ferreira, "The multilevel modular DC converter," *IEEE Trans. Power Electron.*, vol. 28, no. 10, pp. 4460–4471, Oct. 2013.

[9] R. Roopa Sri, & K. Meenendranath Reddy. (2023). Improved Power Management Control of a Multiport Converter Based EV Charging Station with PV and Battery. *International Journal of Research in Science & Engineering* , *3*(02), 16–25.

[10] S. K. Mazumder, A. H. Nayfeh, and D. Boroyevich, "Theoretical and experimental investigation of the fast-scale instability of DC–DC converters," *IEEE Trans. Power Electron.*, vol. 16, no. 2, pp. 201–216, Mar. 2001.

[11] Babburi, S. (2025). Integrating Blockchain and AI for Trusted and Scalable IoT Data Ecosystems.

[12] Bajarang Bhagwat, V. (2023). Optimizing Payroll to General Ledger Reconciliation: Identifying Discrepancies and Enhancing Financial Accuracy. JOURNAL OF ADVANCE AND FUTURE RESEARCH, 1(4). https://doi.org/10.56975/jaafr.v1i4.501636.

[13] M. H. Rashid, *Power Electronics: Circuits, Devices, and Applications*, 4th ed. Upper Saddle River, NJ, USA: Pearson, 2014.

[14] Balaji, A. ., & Reddy, K. M. . (2023). An Interlinking Converter for Renewable Energy Integration into Hybrid Grids. *Journal of Energy Engineering and Thermodynamics*, *3*(02), 12–21.